LETTERS

New Stacking Variations of the Charge and Orbital Ordering in the Metal-Ordered Manganite YBaMn$_2$O$_6$

H. Kageyama[1], T. Nakajima[1], M. Ichihara[1], Y. Ueda[1], H. Yoshizawa[2] and K. Ohoyama[3]

[1]*Material Design and Characterization Laboratory, Institute for Solid State Physics, University of Tokyo, 5-1-5 Kashiwanoha, Kashiwa, Chiba 277-8581*
[2]*Neutron Scattering Laboratory, Institute for Solid State Physics, The University of Tokyo, 106-1 Shirakata, Tokai, Ibaraki 319-1106*
[3]*Institute for Materials Research, Tohoku University, 2-1-1 Katahira, Aoba-ku, Sendai 980-8577*

We performed transmission electron microscopy (TEM) and powder neutron diffraction experiments on an A-site ordered manganese perovskite YBaMn$_2$O$_6$ which undergoes unusual and multiple phase transitions. In the paramagnetic insulating phase, the so-called CE type of charge and orbital ordering was observed in the monoclinic a–b plane, which has been frequently observed for the ordinary solid solution of $A_{1-x}^{3+}A_x'^{2+}$MnO$_3$ around $x = 0.5$. TEM revealed, however, a fourfold periodicity along the c axis, suggesting a new stacking pattern, in which planes of the CE type are built up according to the sequence $[\alpha\alpha\beta\beta\ldots]$. Interestingly, when the system entered the antiferromagnetic state below 195 K, this stacking pattern changed into $[\alpha\alpha\alpha\alpha\ldots]$ or $[\alpha\beta\alpha\beta\ldots]$, suggesting a close interplay between spins and orbitals. The obtained stacking patterns were strongly correlated to the inherent structural alternation, i.e., the Y/Ba order along the c axis.

KEYWORDS: YBaMn$_2$O$_6$, TEM, neutron diffraction, ordered perovskite, charge/orbital order
DOI: 10.1143/JPSJ.72.dummy

Perovskite (ABO_3) and its related compounds (A_2BO_4, $A_3B_2O_7$, etc.) display interesting electric, magnetic and optical properties. Most well-known examples are the high-T_c superconductivity in cuprates ($B = $ Cu)[1] and the colossal magnetoresistance in manganites ($B = $ Mn).[2] Emergence of various interesting phenomena in the perovskite systems is partly due to the versatility of the A site, which forms a wide range of solid solutions between cations with different valences and ionic sizes. This advantage provides us an opportunity to systematically tune the doping level x as well as the Goldschmidt tolerance factor f, as demonstrated by La$_{2-x}$Sr$_x$CuO$_4$ and La$_{1-x}$Ca$_x$MnO$_3$.[3,4]

It should be stressed, however, that such a partial substitution can always be a cause of structural disorder. In $A_{1-x}A_x'$MnO$_3$, the shape, size and tilting angle of each MnO$_6$ octahedron would depend largely on nearby A/A' ions. It means that crystallographic parameters refined using x-ray diffraction (XRD) or neutron diffraction (ND) data correspond only to spatially averaged values. A problem to be addressed is that the randomness of the underlying lattice should affect the physical properties to a certain degree. The effect would become more serious when one deals with microscopic phenomena. It is possible that the structural disorder and spatial heterogeneity trigger or accelerate electronic phase segregation, as recently observed in La$_{2-x}$Sr$_x$CuO$_4$[5] and La$_{0.5}$Sr$_{0.5}$MnO$_3$.[6]

Fortunately, one can obtain a 'clean' system when x in $A_{1-x}^{3+}A_x'^{2+}BO_3$ is 1/2. In Y$_{0.5}$Ba$_{0.5}$CoO$_{3-y}$,[7,8] for example, A-site metal ordering takes place in a way that the YO and BaO layers are built up alternatively. Therefore, the chemical composition should be better denoted as YBaCo$_2$O$_{6-y}$. Recently, we have succeeded in synthesizing its manganese analogue, YBaMn$_2$O$_6$ ($A = $ Y, $A' = $ Ba, $B = $ Mn),[9,10] whose structural and physical properties are considerably different from those of the conventional disordered $A_{0.5}A_{0.5}'$MnO$_3$ system with randomly distributed A/A' ions.[11,12] YBaMn$_2$O$_6$ undergoes unusual phase transitions

as a function of T: a 1st order structural phase transition at $T_{c1} = 520$ K from triclinic $P1$ to monoclinic $P2$, a metal–insulator (MI) transition at $T_{c2} = 480$ K and antiferromagnetic ordering at $T_{c3} = 195$ K. One of the peculiar features is the separation of the structural and MI transition temperatures (i.e., $T_{c2} \neq T_{c1}$), which is strikingly in contrast to the $A_{0.5}A_{0.5}'$MnO$_3$ system, where these transitions occur simultaneously (i.e., $T_{c1} = T_{c2}$). Also interesting is the fact that the value of T_{c2} is, to the authors knowledge, the highest in the manganese perovskite family.

Structural considerations[9,10] indicate that these unusual properties in YBaMn$_2$O$_6$ are attributable to (1) the absence of lattice disorder, (2) the two-dimensionality due to the stacking sequence of –YO–MnO$_2$–BaO–MnO$_2$–, and (3) the MnO$_6$ octahedron distorted heavily from the rigid one. However, to fully understand the correlation between the structural and physical properties, it is necessary to understand how the charge, orbital and spin degrees of freedom crystallize on cooling. In this study, we performed experiments of transmission electron microscopy (TEM) and powder ND for the paramagnetic insulating phase (PI; $T_{c3} < T < T_{c2}$) and the antiferromagnetic insulating phase (AFI; $T < T_{c3}$). It was found that the obtained charge and orbital ordering (COO) pattern in the PI phase differs from that for the disordered $A_{0.5}A_{0.5}'$MnO$_3$ systems. Interestingly enough, the antiferromagnetic long-range ordering at T_{c3} redesigns the COO pattern.

A polycrystalline sample of YBaMn$_2$O$_6$ was prepared by a conventional solid state reaction as reported in ref. 9. Superlattices produced by COO were probed by TEM (JOEL EM2010) operated at 200 kV, using a low-T sample holder, which is controllable from room temperature (RT) down to 24 K. The sample was finely ground in methanol and then was placed on Cu microgrid meshes for TEM observation. Powder ND experiments, which allow us to determine the magnetic ordering, were conducted for 25 K $< T <$ 350 K using the Kinken powder diffractometer for high-efficiency

and high-resolution measurements, HERMES, at the Institute for Materials Research (IMR), Tohoku University, installed at the JRR-3M reactor in the Japan Atomic Energy Research Institute (JAERI), Tokai. Neutrons with a wavelength of 1.8196 Å were obtained by the 331 reflection of the Ge monochromator. The 12′-blank-sample-22′ collimation was employed.

Shown in Fig. 1 is the crystal structure of $YBaMn_2O_6$ at 350 K (the PI phase), determined from the Rietveld refinement of both powder XRD and ND patterns. The details of the structural analysis will be reported elsewhere.[10] The structure of the PI phase adopts a monoclinic space group $P2$ with a unit cell dimension of $\sqrt{2}a_p \times \sqrt{2}b_p \times 2c_p$, where a_p, b_p and c_p denote the cell constants for the simple cubic perovskite. The analysis of the powder ND data for 350 K gave lattice parameters of $a = 5.5193(3)$ Å, $b = 5.5131(3)$ Å, $c = 7.6135(2)$ Å, and $\beta = 90.295(3)°$. For simplicity, we will use simple cubic perovskite notations (indicated by subscript "p") to discuss the experimental results in the remaining text. The structure contains two crystallographically inequivalent Mn sites, Mn(1) and Mn(2). Viewed along the a_p, b_p and c_p axes, the MnO_6 octahedra are tilted to give trans configurations. Each octahedron is heavily distorted due to the A-site order. There is a significant difference in the volume between two inequivalent MnO_6 octahedra [9.998 Å^3 for Mn(1) and 9.547 Å^3 for Mn(2)], suggesting a charge ordering, where the Mn^{3+} and Mn^{4+} ions occupy the Mn(1) and Mn(2) sites, respectively. In contrast, the structure at 500 K ($T_{c2} < T < T_{c1}$) is very close to that of the PI phase but Mn(1)O_6 and Mn(2)O_6 are similar in size, which is compatible with the metallic conductivity.

Figure 2(a) shows the $[100]_p$-zone TEM image and the corresponding electron diffraction pattern at RT (for the PI phase), which clearly reveal a modulation originating from the alternate stack of the YO and BaO layers along the c
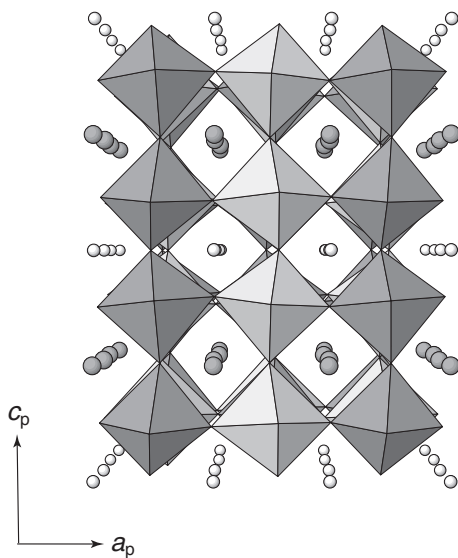

Fig. 1. Perspective view of the crystal structure of the monoclinic $YBaMn_2O_6$ at 350 K (the PI phase) along the $[010]_p$-zone axis, where the Mn(1)O_6 and Mn(2)O_6 octahedra are shown as light and dark polyhedra, respectively, while the Ba^{2+} and Y^{3+} ions are shown by dark and light balls.

axis. The 7.5(4) Å periodicity of the modulation deduced from the TEM image is indeed in good agreement with the ND result [$c = 7.6135(3)$ Å]. The doubling of the c parameter can be confirmed from the electron diffraction pattern, which contains, in addition to the main reflection spots, relatively strong superlattice reflections with a twofold periodicity along $[001]_p$. The high quality and homogeneity of the specimen with the A-site order can be confirmed by the fact that this modulation spreads over a wide range of the TEM image.

In manganite perovskites, various COO states can be directly probed by TEM.[13–15] Figure 2(b) shows the $[001]_p$-zone lattice image taken also at RT. Together with the contrast corresponding to the reduced lattice constants, a_p and b_p (∼3.9 Å), we found an 11.0 Å modulation (q_1) along the $[110]_p$ (or $[1\bar{1}0]_p$) direction.[16] The corresponding superlattice reflections are shown in the inset of Fig. 2(b). This superlattice, represented as $q_1 = (1/4, 1/4, 0)_p$ [or $(1/4, -1/4, 0)_p$], can be ascribed to the so-called CE-type COO in the a–b plane, since the same COO pattern in the a–b plane has been frequently observed for $A_{1-x}A'_x MnO_3$ when x is around 0.5.[13,14] Interestingly, a careful observation of the inset of Fig. 2(a) further reveals very weak reflections, the modulation of which is commensurate and can be denoted as $q_2 = (0, 0, 1/4)_p$. The interlayer COO can explain the q_2 superlattice reflections, which will be discussed later.

It is important to note that the $(1/2, 1/2, 0)_p$ reflection is not a direct consequence of the checkerboard-type charge ordering in the ab plane. It is well known that octahedral tilting distortions, as seen in $GdFeO_3$, allow this reflection. In fact, the Rietveld refinement of the XRD/ND data even in the metallic state above T_{c2} gave the chemical unit cell of $\sqrt{2}a_p \times \sqrt{2}b_p \times 2c_p$.[10] It should also be pointed out that the q_1 and q_2 modulations probed by TEM were invisible from the XRD/ND experiments. This is because the latter experiments were performed with the use of powder samples. The shifts of atomic positions relevant to these structural modulations would be too small to be observed by the powder XRD/ND experiments.

We obtained electron diffraction patterns at RT (the PI state) along various directions and then plotted the observed superlattice reflections on the reciprocal lattice in Fig. 3(a). The most intriguing feature in the present study is the presence of the modulation vector $q_1 = (0, 0, 1/4)_p$. We consider that the origin of the q_1 modulated structure is the stacking sequence of the CE-type layers. There are various methods of piling up the CE-type layers along the c axis so as to satisfy the unit cell $2\sqrt{2}a_p \times \sqrt{2}b_p \times 4c_p$. Figures 4(a) and 4(b) show two possible models, both of which have the stacking sequence along the c axis described by $[\alpha\alpha\beta\beta\ldots]$. In addition, one can conceive more complicated models with stacking sequences such as $[\alpha\beta\gamma\delta\ldots]$ and $[\alpha\alpha\beta\gamma\ldots]$ (not shown). Whatever the appropriate pattern is, we would like to emphasize that it forms a striking contrast to the half-doped solid solution, where a uniformly stacked pattern [Fig. 4(c)], which is in other words, the original 3D CE-COO pattern given by Wollan *et al.*,[17] has always been observed.[13,14]

Among the candidates, the model shown in Fig. 4(a) consists of the uniform alignment of each charge and is consistent with the structure determined by the powder
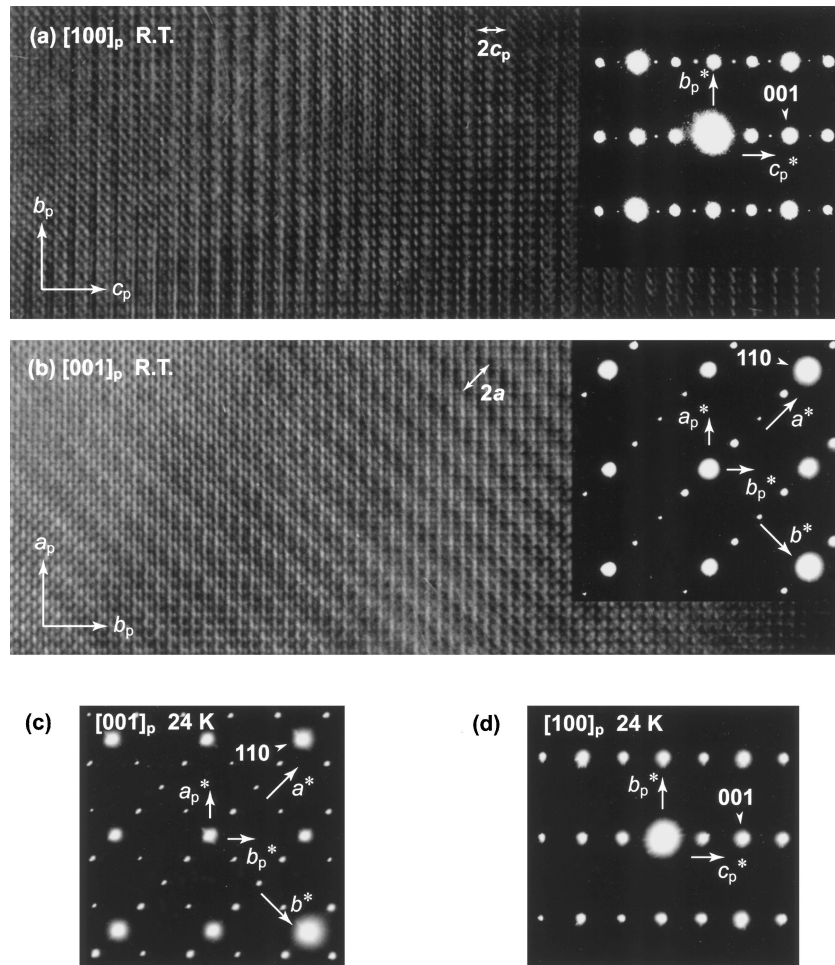
Fig. 2.   High-resolution TEM images and electron diffraction patterns of $YBaMn_2O_6$ at RT obtained along (a) the $[100]_p$-zone and (b) $[001]_p$-zone axes. Electron diffraction patterns at 24 K obtained along (c) the $[001]_p$-zone and (d) $[100]_p$-zone axes.
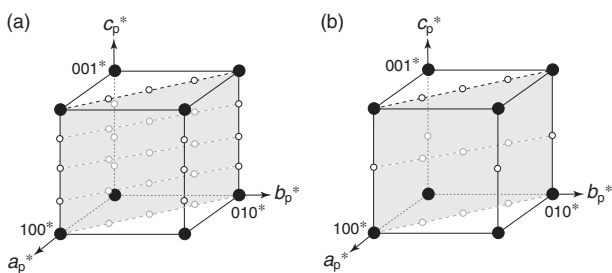

Fig. 3.   Reciprocal lattices with fundamental (closed) and superlattice (open) reflections, obtained from TEM at (a) RT and (b) 24 K.

XRD/ND study.[10] We confirm that the powder XRD/ND patterns, in which the fourfold periodicity was not observed, were analyzed based on the smaller unit cell. However, the refined crystal structure would be almost close to the real one as long as the structural modulations arising from the COO are considerably small. Actually, the obtained structural parameters, such as bond length, Mn–O–Mn bridging angle and so on, are quite reasonable and the reliable factors are as good as those for the higher temperature phases without COO. Of course it is impossible to completely exclude other models from the present study; if one of other models is a relevant model, the Rietveld analysis using the unit cell of $\sqrt{2}a_p \times \sqrt{2}b_p \times 2c_p$ would provide only an averaged structure with larger displacement parameters and possibly with larger reliable factors. In order to confirm the 3D *CE*-COO structure, we may need to perform structural characterization with the use of single crystals, which have not been grown yet.

As stated above, the model in Fig. 4(a), where the $d_{3x^2-r^2}$- and $d_{3y^2-r^2}$-orbitals stack as $[\alpha\alpha\beta\beta\ldots]$, is possibly realized in the PI state. It is interesting to compare this novel stacking sequence $[\alpha\alpha\beta\beta\ldots]$ in $YBaMn_2O_6$ with that in NaV_2O_5.[18] In this layered vanadate, a number of different charge stacking patterns appear in the pressure-temperature phase diagram, which is successfully mapped onto the ANNNI model (devil's staircase). In the manganese perovskite systems, however, the most probable key in determining the 3D *CE*-type COO structures lies in the *A*-site order/ disorder. In the case of $A_{0.5}A'_{0.5}MnO_3$, the interlayer *orbital* interaction that governs the stacking form is uniform. Depending on the sign of the *orbital* interaction, we can deduce two possible superstructures, $[\alpha\alpha\alpha\alpha\ldots]$ and $[\alpha\beta\alpha\beta\ldots]$, shown in Figs. 4(c) and 4(d), respectively, though the real system favors the former as mentioned above. On the contrary, the interlayer *orbital* interactions for $YBaMn_2O_6$ can be alternated since each MnO_2 layer is sandwiched by different layers (i.e., the YO and BaO layers) with considerably different ionic radii ($r_{Y^{3+}} = 1.18\,\text{Å}$, $r_{Ba^{2+}} = 1.61\,\text{Å}$). The $[\alpha\alpha\beta\beta\ldots]$ proposed pattern [Fig.
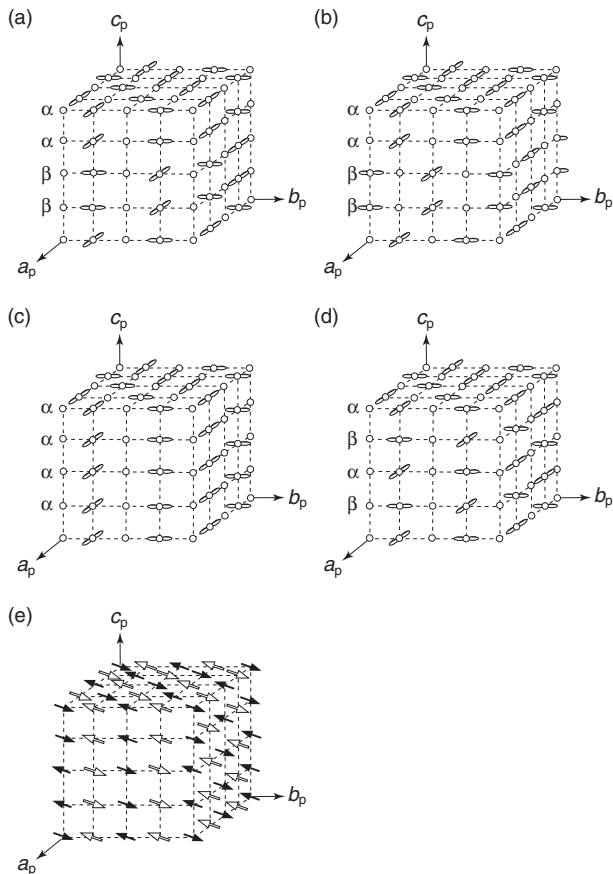
Fig. 4. Various COO patterns (a)–(d) and a spin-ordering pattern (e), where for simplicity only Mn^{3+} and Mn^{4+} ions are drawn. (a) and (b): possible COO structures for the PI phase with the fourfold periodicity along the *c* axis. In each case, we have to determine the proper location of the BaO (or YO) layers: the BaO (or YO) layers are intervened either between out-of-phase planes (i.e., $\alpha\beta$) or in-phase planes (i.e., $\alpha\alpha$ and $\beta\beta$). (c) and (d): possible COO structures for the AFI phase. It is noted that the model (c) having uniform stacking is the original 3D *CE*-type COO structure and is obtained for the metal-disordered $A_{0.5}A'_{0.5}MnO_3$ system.
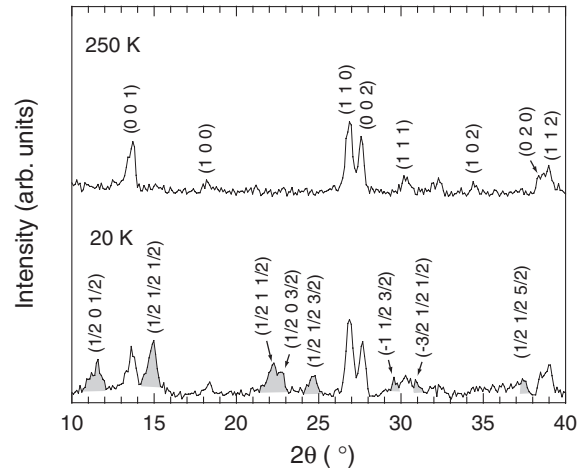

Fig. 5. ND profiles of $YBaMn_2O_6$ at 250 K and 20 K, where the peaks are indexed according to the $\sqrt{2}a_p \times \sqrt{2}b_p \times 2c_p$ unit cell.

4(a)] is naturally explained if the sign of the interlayer *orbital* interactions changes alternatively. So far we do not have any microscopic picture of the interlayer *orbital* interaction. Clarifying the mechanism, qualitatively or quantitatively, calls for further investigation. It is noteworthy that another model with the sequence of $[\alpha\alpha\beta\beta\ldots]$ [Fig. 4(b)] can be similarly understood in terms of the Y/Ba ordering and the interlayer coulomb interaction, while other complicated models cannot.

Finally, we would like to discuss the superstructure in the AFI state below T_{c3}. Figure 5 compares the ND patterns taken at 250 K and 20 K. While all of the peaks for the PI phase are of nuclear origin and can be indexed by assuming a monoclinic symmetry with the $\sqrt{2}a_p \times \sqrt{2}b_p \times 2c_p$ unit cell, additional peaks of magnetic origin appear when $T < T_{c3}$. It is revealed from indexing these magnetic peaks that the spin-ordering pattern in the *a–b* plane is the same as that observed in $A_{0.5}A'_{0.5}MnO_3$,[19] but that along the *c* axis has a fourfold periodicity. The proposed spin structure is shown in Fig. 4(e). Such a quadruplication along the *c* axis has not been observed for the $A_{0.5}A'_{0.5}MnO_3$ system because it is uniquely determined that the interlayer magnetic

interaction is ferromagnetic. Again, it is quite natural to consider that the Y/Ba order along the *c* axis in $YBaMn_2O_6$ makes the interlayer magnetic interactions alternated between ferro- and antiferromagnetic, resulting in the proposed spin structure.

The electron diffraction pattern at 24 K [Fig. 2(c)] is interpreted as the superimposition of twin domains both of which have the q_1 modulation. This implies that the *CE*-type COO is retained within the *a–b* plane. Figure 2(d) shows, interestingly enough, the disappearance of the modulation vector q_2 in the AFI state, although the system still has the fourfold periodicity due to the spin ordering. The superlattice reflections at 24 K obtained by TEM are summarized in Fig. 3(b) and possible models of the COO are depicted in Figs. 4(c) and 4(d), where layers of the *CE*-type COO are piled up according to $[\alpha\alpha\alpha\alpha\ldots]$ and $[\alpha\beta\alpha\beta\ldots]$, respectively. The change of the 3D superstructures of the COO strongly suggests the keen competition between the *orbital* and magnetic interactions. The observed rearrangement across T_{c3} is partly supported by the nature of a 1st-order phase transition (relatively large hysteretic behavior in the magnetic susceptibility and heat absorption/release observed in a differential scanning calorimetry (DSC) measurement).[9]

To summarize, we have investigated the superstructures of $YBaMn_2O_6$ in the charge-, orbital- and spin-ordered states by TEM and ND experiments. In the PI phase, in addition to the superlattice reflections originating from the *A*-site metal order, novel superlattice reflections with modulation vectors $q_1 = (1/4, 1/4, 0)_p$ and $q_2 = (0, 0, 1/4)_p$ appear. These modulations are interpreted as the *CE*-type COO in the *a–b* plane and its stacking arrangement along the *c* axis. It should be stressed that the stacking sequence according to $[\alpha\alpha\beta\beta\ldots]$ was first observed among partially doped manganese perovskite compounds. In the AFI phase, we observed the disappearance of q_2, indicating the uniform $[\alpha\alpha\alpha\alpha\ldots]$ or alternative $[\alpha\beta\alpha\beta\ldots]$ stacking of the *CE*-type COO layers along the *c* axis. Transformation of the COO would be mediated by the spin ordering with a quadruplicate periodicity along the same axis.

1) J. G. Bednorz and K. A. Muller: Z. Phys. B **64** (1986) 189.
2) S. Jin, T. H. Tiefel, M. Mccormack, R. A. Fastnacht, R. Ramesh and L. H. Chen: Science **264** (1994) 413.
3) G. M. Luke *et al.*: Phys. Rev. B **42** (1990) 7981.
4) C. Martin, A. Maignan, M. Hervieu and B. Raveau: Phys. Rev. B **60** (1999) 12191.
5) J. M. Tranquada, B. J. Sternlieb, J. D. Axe, Y. Nakamura and S. Uchida: Nature **375** (1995) 561.
6) S. Mori, C. H. Chen and S.-W. Cheong: Phys. Rev. Lett. **81** (1998) 3972.
7) W. Z. Zhou: Chem. Mater. **6** (1994) 441.
8) D. Akahoshi and Y. Ueda: J. Phys. Soc. Jpn. **68** (1999) 736.
9) T. Nakajima, H. Kageyama and Y. Ueda: J. Phys. Chem. Solids **63** (2002) 913.
10) T. Nakajima *et al.*: preprint.
11) P. M. Woodward, T. Vogt, D. E. Cox, A. Arulraj, C. N. R. Rao, P. Karen and A. K. Cheetham: Chem. Mater. **10** (1998) 3652.
12) *Colossal Magnetoresistance, Charge Ordering and Related Properties of Manganese Oxides*, ed. C. N. R. Rao and B. Raveau (World Scientific, Singapore, 1998).
13) Y. Q. Wang, X. F. Duan, Z. H. Wang and B. G. Shen: Mater. Sci. Eng. A **333** (2002) 80.
14) N. Fukumoto, S. Mori, N. Yamamoto, Y. Moritomo, T. Katsufuji, C. H. Chen and S.-W. Cheong: Phys. Rev. B **60** (1999) 12963.
15) T. Asaka, S. Yamada, S. Tsutsumi, C. Tsuruta, K. Kimoto, T. Arima and Y. Matsui: Phys. Rev. Lett. **88** (2002) 097201.
16) For both PI and AFI states, we usually observed microtwinstructures with the modulations, $(1/4, 1/4, 0)_p$ and $(1/4, -1/4, 0)_p$ [see Fig. 3(c)]. Note that one cannot identify the *a* and *b* axes from the [001] electron diffraction patterns because of the nearly tetragonal chemical unit cell (i.e., $a_p \cong b_p$, $\beta \cong 90°$).
17) E. O. Wollan and W. C. Koehler: Phys. Rev. **100** (1955) 545.
18) K. Ohwada, Y. Fujii, N. Takesue, M. Isobe, Y. Ueda, H. Nakao, Y. Wakabayashi, Y. Murakami, K. Ito, Y. Amemiya, H. Fujihisa, K. Aoki, T. Shobu, Y. Noda and N. Ikeda: Phys. Rev. Lett. **87** (2001) 086402.
19) Z. Jirák, F. Damay, M. Hervieu, C. Martin, B. Raveau, G. André and F. Bourée: Phys. Rev. B **61** (2000) 1181.